arXiv:1208.0299v1 [cond-mat.soft] 1 Aug 2012

Dynamic crossover length in soft-glassy materials

R.Benzi [1], M. Bernaschi [2], M. Sbragaglia [1] and S. Succi [2]
[1] Department of Physics and INFN, University of "Tor Vergata", Via della Ricerca Scientifica 1, 00133 Rome, Italy
[2] Istituto per le Applicazioni del Calcolo CNR, Via dei Taurini 19, 00185 Rome, Italy

Based upon mesoscale simulations of binary mixtures with very low surface tension and positive disjoining pressure (frustration), we measure the correlation length of the stress field within the flowing mixture, as a function of the frequency of the applied load. Two scaling regimes are clearly identified, with a sharp crossover between the liquid and solid regions, with exponent $-1/2$ and -1, respectively. The crossover correlation length is shown to be closely connected to the typical scale of the coherent excitations of the density field, whose collective dynamics is shown to be responsible for non-trivial rheological effects including the emergence of yield stress.

PACS numbers: 47.50.Cd,47.11.St,87.19.rh,83.60.Rs

INTRODUCTION

Soft-Glassy (SG) materials exhibit features of both liquid and solid states of matter [1, 2], and consequently they present a major challenge to standard concepts and tools of thermodynamics and non equilibrium statistical mechanics [4–18]. Despite their disparate physico-chemical nature, such materials share several generic features, primarily an anomalous relaxation time to equilibrium and a non-linear relation between the applied stress and the resulting strain rate (non-Newtonian rheology). This behaviour is sometimes accompanied by a so called yield-stress, i.e. a minimum stress threshold, below which the material does not flow, showing solid-like behaviour [8]. The microscopic roots of such an intriguing rheology have made the object of intense scrutiny in the recent years, via molecular dynamics simulations [17], mesoscopic models [7, 9, 18], as well as experimental work [4, 5, 8, 16]. Although much has been learned thanks to these efforts, a commonly agreed theoretical picture is yet to emerge [9, 11, 13].

An important question which underlies the aforementioned phenomenology concerns the basic mechanisms controlling the crossover from liquid to solid-like behaviour of SG materials. In particular, in this Letter, we exhibit evidence that there exists a *dynamic crossover scale*, l_{DCS}, marking the transition between the two regimes, i.e., phenomena correlating below (above) l_{DCS} are classified as liquids (solids). We propose a well-defined operational procedure to measure this characteristic length-scale, based on the spatial correlation of the velocity (stress) field. It is reasonable to expect that such correlation length-scale bears a link with other length-scales discussed in the literature, namely the shear transformation zones [19] and cooperative length-scales [7]. In our work we employ a mesoscopic model of binary fluid, where a suitable frustration mechanism at the interface is introduced by combining a small positive surface tension, promoting highly complex interfaces, with a positive disjoining pressure, inhibiting interface coalescence. The mesoscopic kinetic model considers a binary mixture of fluids A and B, each described by a discrete kinetic Boltzmann distribution function $f_s(\vec{r},\vec{v}_i,t)$, measuring the probability of finding a representative particle of fluid $s=A,B$ at position $\vec{r}$ and time t, with discrete velocity $\vec{v}_i$, where the index i runs over the nearest and next-to-nearest neighbors of $\vec{r}$ in a regular two-dimensional lattice [20]. By definition, the mesoscale particle represents all molecules contained in a unit cell of the lattice. The distribution functions of the two fluids evolve under the effect of free-streaming and local two-body collisions, described by a momentum-relaxation to a local equilibrium ($f^{(eq)}$) on a time scale τ for both fluids ($s=A,B$):

$$f_s(\vec{r}+\vec{v}_i,\vec{v}_i,t+1)-f_s(\vec{r},\vec{v}_i,t)= \\ -\frac{1}{\tau}\left(f_s-f_s^{(eq)}\right)(\vec{r},\vec{v}_i;t)+F_s(\vec{r},\vec{v}_i;t).$$

The term $F_s(\vec{r},\vec{v}_i,t)$ includes a variety of interparticle forces. First, a repulsive force with strength parameter $\mathcal{G}_{AB}$ between the two fluids ensures phase separation [20] (see triangles in figure 1). Furthermore, both fluids are also subject to short range self-attraction (controlled by strength parameters $\mathcal{G}_{AA,1}<0$, $\mathcal{G}_{BB,1}<0$), and mid-range self-repulsion (regulated by strength parameters $\mathcal{G}_{AA,2}>0$, $\mathcal{G}_{BB,2}>0$). In this way, one has the basic ingredients for ideal phase separation plus forces within each species whose role is twofold. First, they set the desired non-ideal (excess) pressure in the bulk. Second, they introduce an effective "long-range" repulsion between the two species which frustrates phase separation. Despite their inherent microscopic simplicity, such dynamic rules are able to promote a host of non-trivial collective effects [20, 21]. Most notably, whenever the self-specie attraction ($\mathcal{G}_{ss,1}$) and repulsion effects ($\mathcal{G}_{ss,2}$) come close to an exact balance, two distinctive phenomena take place: low surface tension is achieved, thus producing a large interface between the two fluids, and a positive disjoining pressure, inhibiting coalescence of the bulk phases. This is what we call *frustration* in our model. The emergence of a positive disjoining pressure

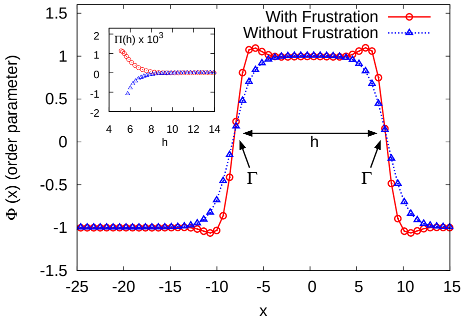

FIG. 1: The order parameter of a thin film composed of two non ideal interfaces separated by a distance h. Each interface is characterized by a surface tension Γ. The order parameter is defined as $\phi = \pm 1$ in the A(B) bulk phase and $\phi = 0$ at the interface location. Two cases are considered: (a) a mixture with purely repulsive fluids; (b) the same mixture plus a *frustration* mechanism. The presence of frustration at the interface translates into a positive disjoining pressure $\Pi(h)$ as the film gets thinner (see inset).

$\Pi(h)$ is shown in figure 1, where we consider a thin *film* with two non ideal interfaces, separated by the distance h [28]. Following Bergeron [22], we write the relation for the corresponding tensions following the Gibbs-Duhem relation:

$$\Gamma_f(h) = 2\Gamma + \int_{\Pi(h=\infty)}^{\Pi(h)} h \, d\Pi \tag{1}$$

where Γ is the bulk value of the surface tension and Γ_f is the overall film tension, whose expression is known in terms of the mismatch between the normal and tangential components of the pressure tensor [23, 24], $\Gamma_f = \int_{-\infty}^{+\infty} (P_N - P_T(x))dx$, where, in our model, $P_N - P_T(x) = p_s(x)$ can be computed analytically [25]. With the knowledge of the relation $s(h) = \Gamma_f(h) - 2\Gamma$, the computation of the disjoining pressure is then straightforward: a simple differentiation of $s(h)$ allows us to compute the first derivative of the disjoining pressure, $\frac{ds(h)}{dh} = h\frac{d\Pi}{dh}$. This information, supplemented with the boundary condition $\Pi(h \to \infty) = 0$, allows us to completely determine the disjoining pressure of the film (see figure 1). The diffuse interface profile *emerges* spontaneously from the underlying mesoscopic dynamics, once the strength of the underlying interactions is properly tuned. We wish to remark that the humped-structure at the frustrated interface (see figure 1) would disappear by lifting the tight competition between short-range attraction and mid-range repulsion, thus showing that frustration is indeed essential to reproduce the correct interface physics. In the absence of such a stabilization mechanism, the rheology of the binary mixture would reduce to a plain Newtonian behaviour.

In the following, we turn to the analysis of the basic rheological behaviour of two dimensional emulsion and foam-like fluids, such as those described in figure 2. We perform two different experiments: in the first case (the “full periodic” experiment) the fluid is placed in a square box $L_x \times L_y = 512 \times 512$ with full periodic boundary conditions. A forcing is then applied in the stream-flow direction, say x, with the property $F_x(y) = F_0 \sin\left(\frac{2\pi y}{L_y}\right)$, where the constant F_0 is tuned so as to reproduce for a stationary fully Newtonian case the velocity profile $u_x(y) = U_0 \sin\left(\frac{2\pi y}{L_y}\right)$. When the frustration mechanism is switched on, the velocity profile deviates from the Newtonian prediction. From the averaged velocity in time and in the stream-flow direction we are able to extract the local strain rate, while the stress is provided by the integral of $F_x(y)$. Such local rheological measurement is displayed in figure 3 (circles) and clearly indicates the existence of a yield stress $\sigma_Y \sim 10^{-4}$. This result is consistent with the rheology obtained in a second experiment (the “Couette” experiment) where the system is confined between two walls ($y = 0$, $y = L_y$) with periodic inlet-outlet boundary conditions. The upper boundary is set to a constant velocity, U_W, resulting in a constant aver-

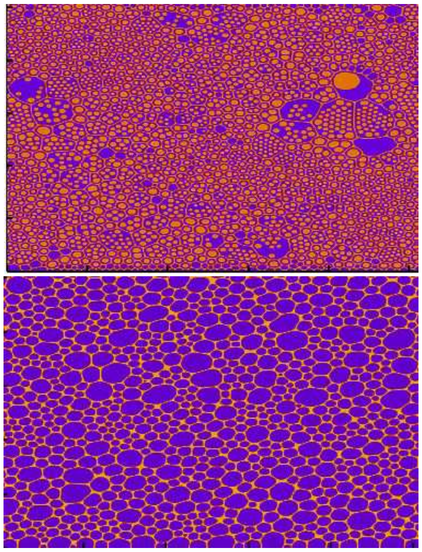

FIG. 2: Typical density configurations in our numerical simulations. We simulate cases with 50:50 (case (a), upper panel) and 30:70 (case (b), lower panel) mass ratio between fluids A and B, respectively. Case (a): we simulate islands of fluid A embedded in fluid B, all entrapped within a ”vesicle” confined by a belt of fluid A. The initial condition is a periodic perturbation of the uniform background density, with wavelength $l_0 = 64$ and zero flow. Case (b): we prepare the system with a collection of polydisperse “packings” of fluid A (B), separated by layers of fluid B and being stabilized by a positive disjoining pressure (see also figure 1). In both cases, the A rich (B rich) region has approximately $\rho_A = 1.2$, $\rho_B = 0.2$ ($\rho_A = 0.2$, $\rho_B = 1.2$). The hydrodynamic viscous ratio between A rich and B rich regions is 1. The coupling parameters are $\mathcal{G}_{AA,1} = -9.0$, $\mathcal{G}_{AA,2} = 8.1$ $\mathcal{G}_{BB,1} = -8.0$, $\mathcal{G}_{BB,2} = 7.1$, $\mathcal{G}_{AB} = 0.587$ and $\rho_0 = 0.83$ [20].

aged stress. The stress-strain rate plot given in figure 3 (squares) reveals that both rheological measurements are in a fairly good agreement. We now turn our attention to the case of a sinusoidal strain applied in the confined Couette experiment. We increase the peak strain amplitude γ and compute the peak stress σ_P, while keeping constant the oscillation frequency $\omega = 10^{-4}$, in line with the analysis reported by Mason & coworkers [3]. The results are shown in the upper inset of figure 3. A power law in the peak stress-strain relation, $\sigma_P \sim \gamma$, is observed for the lower strains. For large γ, the system starts to yield and the peak stress exhibits a sub-linear power law behaviour, as observed in [3] and the yield stress σ_Y is, within a factor 2, consistent with the one obtained in the main plot of figure 3. Next, we investigate the response of the system when the upper boundary is oscillating according to the relation $u_W(t) = U_W\, cos(\omega t)$, with ω the load frequency and $U_W = 0.001$. Notice that the strain is now function of ω, i.e. $\gamma \sim U_W/\omega$. In this setup, the stress is typically expressed as $\sigma(t) = G'(\omega)\sin(\omega t) + G''(\omega)\cos(\omega t)$, where G' is the storage modulus and G'' is the loss modulus. In the bottom insert of figure 3 we show G' and G'' as a function of ω. In typical SG materials, say concentrated emulsions, there is a prevalence of G', up to a crossover frequency, where the fluid component G'' takes over. It is apparent, looking at the inset, that $G'(\omega)$ (solid response) prevails over $G''(\omega)$ (liquid response) at all frequencies up to $\omega \sim 5-8\times\ 10^{-3}$.

The main goal of the present letter is to investigate the physics of spatial structures responsible for the complex and non linear rheology described in figure 3. To this purpose we consider the *spatial* stress correlator:

$$C_\sigma(y) = \frac{\langle \sigma(L_y,t)\ \sigma(y,t)\rangle}{\langle \sigma^2(L_y,t)\rangle^{1/2}\langle \sigma^2(y,t)\rangle^{1/2}} \qquad (2)$$

where $\sigma(y,t)$ denotes the averaged stress in the stream-flow direction and the brackets denote time average (typically over 10^6 time-steps). In a liquid system with viscosity ν_N, the fluid velocity $u_x(y,t)$, averaged in the stream-flow direction, oscillates in time with frequency ω and decays as $e^{-(L_y-y)/l_f}$, where $l_f \sim \sqrt{\nu_N/\omega}$. As a consequence, the stress $\sigma(y,t)$ shows the same behavior and the stress correlation (2) behaves as $C_\sigma(y) = \cos(2\pi(L_y-y)/l_f)$. In a solid-elastic system, we expect $C_\sigma(y) = \cos(2\pi(L_y-y)/l_s)$, where $l_s \propto c_s/\omega$, c_s being the sound speed. Thus we conclude that, in our system, as well as in many other SG systems, the correlator can be written as $C_\sigma(y) = \cos(2\pi(L_y-y)/l(\omega))$. As a result, we can use the scaling $l(\omega)$ *vs* ω to quantitatively assess the transition from liquid- to solid-like behavior. Notice that the computation of $l(\omega)$ can be carried out only for large enough L_y, *i.e.* when inertial effects become important. In figure 4, we report the results for $l(\omega)$, as extracted from the *spatial* stress correlator $C_\sigma(y)$ in a domain of size $L_x = 1024$ and $L_y = 1024$ for the setup of case (a) of figure 2 (results related to the setup of case (b) are presented in figure 5). The wall speed is fixed to $U_W = 0.001$, whereas the load frequency is varied in the range $10^{-4} < \omega < 10^{-2}$. The simulation data provide a very neat indication of the two regimes, with exponents $-1/2$ and -1, respectively. Moreover, a sharp cross-over between the two regimes is clearly observed at a crossover frequency $\omega_c \approx 3\times\ 10^{-3}$, which identifies a correlation length, $l_{DCS} \approx 100$, in lattice units. This length is of the order of a few l_0 (see caption of figure 2), i.e. a few times the characteristic size of the density wavelength in the initial condition, indicating that the collective excitations of the density field in the solid-like phase are basically lumps of fluid within a given belt, surrounded by their nearest neighbors. We also repeated the numerical simulations for the case of a fluid without liquid-liquid repulsion $\mathcal{G}_{AB} = 0$, thus recovering the Newtonian behaviour for a homogeneous fluid. Consistently with expectations, we note that the liquid scaling (squares) extends all the way into the low frequency region. A possible way to rephrase the results of figure 4, is to define a frequency-dependent effective viscosity, $\nu_{eff}(\omega) = \omega\, l^2(\omega) \approx c_s^2/\omega$, that highlights the divergence of the viscosity in the low-frequency limit $\omega \to 0$. In the inset of figure 4 we show $\nu_{eff}(\omega)/\nu_N$ as a function of ω, where ν_N corresponds to the Newtonian viscosity obtained for $\mathcal{G}_{AB} = 0$. In the same inset, we plot the peak stress σ_P normalized with respect to the corresponding Newtonian value. Both ν_{eff} and σ_P increase as $1/\omega$ for small ω, which is consistent with the interpretation of $\omega l^2(\omega)$ as an effective viscosity. Let us remark that, in a Newtonian liquid, $\sigma_P \sim \nu_N U_W/L_y$ should be independent of ω whereas in a solid-elastic system σ_P is proportional to $1/\omega$. The picture emerging from our results is that the fluid behaves like a liquid at short-scales, where the leading equilibration mechanism is the local relaxation in momentum space, and like an amorphous solid at large scales, where the correlated dynamics of the collective degrees of freedom undergoes anomalous slow-down, with an ensuing substantial increase of the viscosity (slow relaxation in configuration space).

An important point is to investigate whether the notion of l_{DCS} may be related to the existence of yield stress σ_Y. Following [3] and our interpretation of l_{DCS}, we argue that σ_Y should be given by the ratio of the surface tension Γ and l_{DCS}. In our case, $\Gamma \sim 10^{-2}$ suggesting $\sigma_Y \sim 10^{-4}$ in agreement with the basic rheological results shown in figure 3. To gain a deeper physical insight, we consider a bi-liquid emulsion system with monodisperse distribution of droplets sizes (see case (b) in figure 2) within a confined Couette geometry with upper wall velocity U_W constant in time. Next, we perform different experiments by varying the nominal shear $S = U_W/L_y$ and compute the average stress $\langle\sigma\rangle$ and the stress correlation function (2) at the channel center $y = L_y/2$. In the inset of figure 5, we show three cases of $C_\sigma(y)$ obtained for different values of S. For each $C_\sigma(y)$ we can estimate

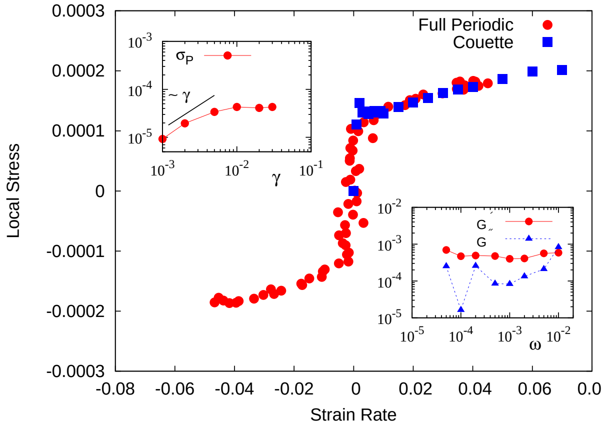

FIG. 3: Basic rheological properties for the soft-glassy configuration of case (a) in Figure 2, see text for details. In the upper inset we report the peak stress σ_P produced by applying a sinusoidal strain with peak amplitude γ at a given frequency $\omega = 10^{-4}$. Shown in the lower inset, is the behaviour of $G'(\omega)$ and $G''(\omega)$, where G' is the storage modulus and G'' is the loss modulus.

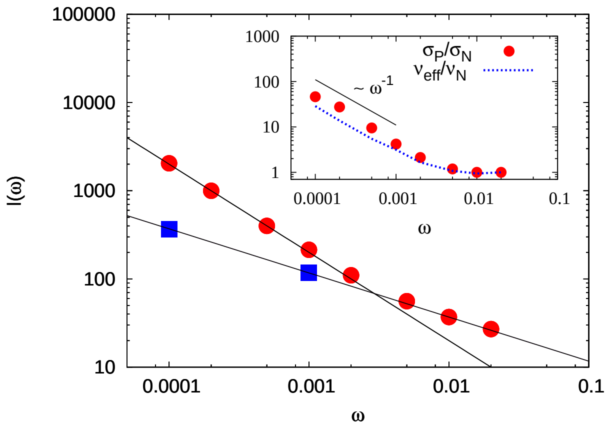

FIG. 4: Stress correlation length as a function of the load frequency. The two straight lines refer to slopes -1 (solid behavior) and $-1/2$ (liquid behavior). The dynamic cross over length is estimated to be $l_{DCS} \sim 100$. The squares refer to the Newtonian case (i.e. $\mathcal{G}_{AB} = 0$) which follows the slope $-1/2$. Inset: we report the effective viscosity $\nu_{eff} = \omega l^2(\omega)$ and the peak stress σ_P normalized to their Newtonian values. For small ω, both quantities show the behavior $1/\omega$.

the decay length l_d as $C_\sigma(L_y/2 \pm l_d) = e^{-1}$. Finally, in the main plot of figure 5, we show $\langle\sigma\rangle$ as a function of l_d/l_{DCS}. If our interpretation of $\sigma_Y \sim \Gamma/l_{DCS}$ is correct, we expect that $\langle\sigma\rangle/\sigma_Y > 1$ for $l_d \approx l_{DCS}$, which is exactly what we observe. The physical meaning of our results implies that the condition required to set the system in motion (*i.e.* for $\langle\sigma\rangle > \sigma_Y$) is that the characteristic fluctuations should be correlated at relatively small scale, *i.e.* smaller than l_{DCS}. In summary, the physical meaning of l_{DCS} appears to be consistent with the solid/liquid transition and the existence of a yield stress. Based on the observations prompted by mesoscale simulations of a binary mixture with competing attractive/repulsive interactions, in this paper we have proposed an operational procedure to identify a typical scale separating fluid-like and solid-like behaviour. Our approach can be tested in laboratory experiments, similar to those recently discussed in [12]. Our model provides a remarkable blend of conceptual simplicity (all interactions are prescribed in terms of elementary lattice interactions) and computational efficiency [29].

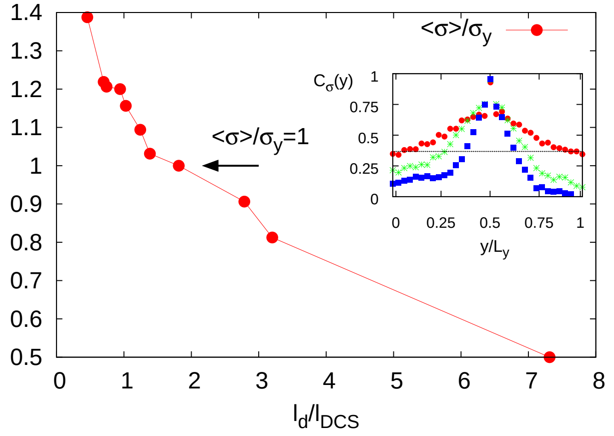

FIG. 5: Average stress (normalized with the yield stress) versus the decay length l_d normalized with l_{DCS}. Data refer to a Couette experiment (see also figure 3) at different nominal shears $S = U_W/L_y$ for a bi-liquid emulsion system with monodisperse distribution of droplets sizes (see case (b) in figure 2). The inset shows the profiles of the stress correlator for three cases: $U_W = 0.005$ (circles), $U_W = 0.01$ (stars), $U_W = 0.04$ (squares), while L_y is kept fixed.

M.S. acknowledges ERC-DROEMU c.n. 279004 for support.

---

[1] R. G. Larson, The Structure and Rheology of Complex Fluids (Oxford University Press, New York, 1999)
[2] P. Coussot, Rheometry of Pastes, Suspensions, and Granular Materials (Wiley-Interscience, Chichester, 2005)
[3] T.G. Mason, J. Bibette & D. A. Weitz, *Jour. Colloid Inter. Science* **179**, 439-448 (1996)
[4] G. Katgert, B. P. Tighe, M. E. Mobius & M. Van Hecke, *Europhys. Lett.* **90**, 54002 (2010)
[5] G. Katgert, A. Latka, M. E. Mobius & M. Van Hecke, *Phys. Rev. E* **79**, 066318 (2009)
[6] L. Becu, S. Manneville & A. Colin, *Phys. Rev. Lett.* **96**, 138302 (2006)
[7] L. Bocquet, A. Colin & A. Ajdari, *Phys. Rev. Lett.* **103**, 036001 (2009)
[8] J. Goyon, A. Colin, G. Ovarlez, A. Ajdari & L. Bocquet, *Nature* **454**, 8487 (2008); J. Goyon, A. Colin & L. Boc-

quet, *Soft Matter* **6**, 2668-2678 (2010)

[9] V. Mansard, A. Colin, P. Chauduri & L. Bocquet, *Soft matter* **7**, 5524 (2011)

[10] G. Ovarlez, S. Rodts, X. Chateau & P. Coussot, *Rheol. Acta* **48**, 831844 (2009)

[11] S. M. Fielding, M. E. Cates & P. Sollich, *Soft Matter* **5**, 23782382 (2009)

[12] V. Chikkadi, G. Wegdam, D. Bonn, B. Nienhuis & P. Schall, *Phys. Rev. Lett.* **107**, 198303 (2011)

[13] P. Schall & M. Van Hecke, *Annu. Rev. Fluid. Mech.* **42**, 67-88 (2010)

[14] K. Krishan & M. Dennin, *Phys. Rev. E* **78**, 051504 (2008)

[15] G. Debregeas, H. Tubuteau & J.M. Di Meglio, *Phys. Rev. Lett.* **87**, 178305 (2001)

[16] D.T.N. Chen, Q. Wen, P.A. Janmey, J.C. Crocker & A. G. Yodh, *Annual Review of Condensed Matter Physics* **1**, 301-322 (2010)

[17] W. Kob & H.C. Andersen, *Phys. Rev. E* **52**, 4134 (1995); F. Varnik, L. Bocquet, J.-L. Barrat & L. Berthier, *Phys. Rev. Lett.* **90**, 095702 (2003); F. Varnik, L. Bocquet & J.-L. Barrat, *J. Chem. Phys.* **120**, 2788 (2004)

[18] P. Sollich P. et al., *Phys. Rev. Lett.* **78**, 2020 (1997); P. Sollich, *Phys. Rev. E* **738**, 58 (1998)

[19] J. S. Langer & A. Lematre, *Phys. Rev. Lett.* **94**, 175701 (2005)

[20] R. Benzi, M. Sbragaglia, S. Succi, M. Bernaschi & S. Chibbaro, *J. Chem. Phys.* **131**, 104903 (2009)

[21] R. Benzi, M. Bernaschi, M. Sbragaglia & S. Succi, *Europhys. Lett.* **91**, 14003 (2010)

[22] V. Bergeron, *J. Phys.: Condens. Matter* **11** R215 (1999)

[23] B. V. Derjaguin, Theory of Stability of Colloids and Thin Films, Transl. R K Johnston (New York: Consultants Bureau, 1989)

[24] B.V. Toshev, *Current Opinion in Colloid & Interface Science* **13**, 100 106 (2008)

[25] X. Shan, *Phys. Rev. E* **77**, 066702 (2008)

[26] C.E. Colosqui, M. E. Kavousanakis, A. G. Papathanasiou & I. G. Kevrekidis, *ArXiv* 1202.6130v1 (2012).

[27] R. Benzi, M. Bernaschi, L. Rossi, M. Sbragaglia & S. Succi, *Phys. Rev. E* **80**, 066707 (2009).

[28] The link between the competing interactions and a tunable disjoining pressure has already been invoked by Colosqui et al. for fluid-solid interactions [26]

[29] Each simulation, spanning multi-million time steps for every single set of parameters, takes about 30 hours on a 2050 Nvidia-GPU. The 2050 Nvidia-GPU features 448 cores grouped in 14 Streaming Multiprocessors running at 1.15 GHz. The code relies on the CUDA 4.0 and offers a speedup in excess of one order of magnitude with respect to a highly tuned (multi-core) CPU version [27]

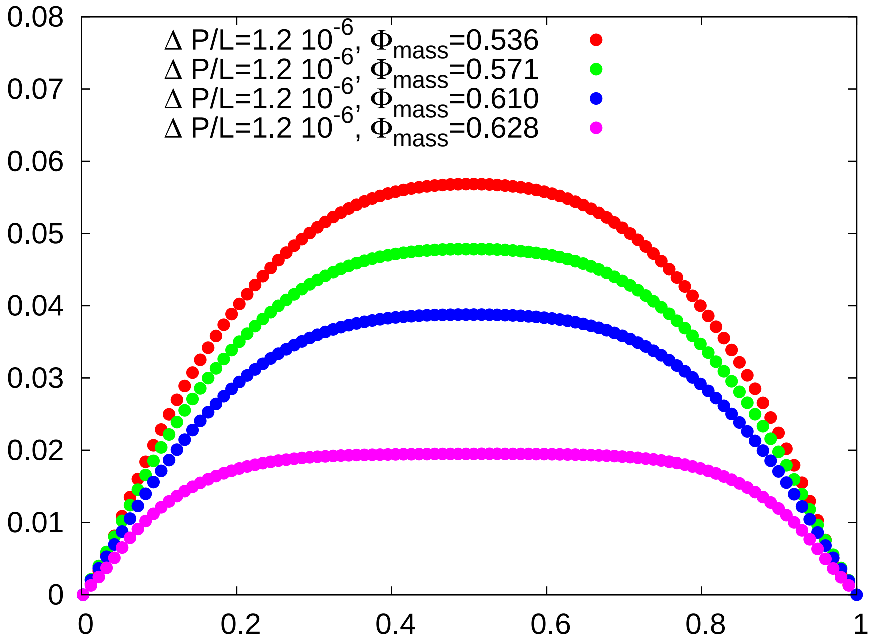

0.08
0.07
0.06
0.05
0.04
0.03
0.02
0.01
0
0
0.2
0.4
0.6
0.8
1
Δ P/L=1.2 10^{-6}, Φ_{mass}=0.536 ●
Δ P/L=1.2 10^{-6}, Φ_{mass}=0.571 ●
Δ P/L=1.2 10^{-6}, Φ_{mass}=0.610 ●
Δ P/L=1.2 10^{-6}, Φ_{mass}=0.628 ●